ELSEVIER

Marine Geology 152 (1998) 247–259

MARINE GEOLOGY
INTERNATIONAL JOURNAL OF MARINE GEOLOGY, GEOCHEMISTRY AND GEOPHYSICS

Magnetic stratigraphy and sedimentology of Holocene glacial marine deposits in the Palmer Deep, Bellingshausen Sea, Antarctica: implications for climate change?

Matthew E. Kirby [a,*], Eugene W. Domack [b], Charles E. McClennen [c]

[a] *Department of Geology, Syracuse University, Syracuse, NY, USA*
[b] *Department of Geology, Hamilton College, Clinton, NY, USA*
[c] *Department of Geology, Colgate University, Hamilton, NY, USA*

Received 27 October 1997; accepted 7 April 1998

Abstract

The Palmer Deep is a closed bathymetric depression on the Antarctic Peninsula continental shelf. It contains three separate sub-basins. These basins lie along a northeast–southwest axis with water depths ranging from >1400 m to the southwest (Basins II and III) to just over 1000 m to the northeast (Basin I). Six sediment piston cores were collected from the study region; these cores clearly demonstrate the varied sediment character for each basin. Sediments in Basin I are laminated and thinly bedded consisting of diatomaceous, pelagic/hemipelagic sediments, siliciclastic, terrigenous sediments, and ice rafted, hemipelagic sediments. In concurrence with other investigators, we propose that these laminations and thin beds represent climatically forced productivity cycles. Basin II and Basin III sediments alternate between pelagic/hemipelagic units and bio-siliceous mud turbidites. Correlations between cores are based on their remarkable magnetic susceptibility (MS) records which indicate alternating biogenic (low MS) and siliciclastic (high MS) dominated sedimentation; the bio-siliceous mud turbidites are characterized by intermediate to low MS values. Cores taken from within the main axis of the basins are expanded ultra-high resolution sections. A core collected on the sill between Basins II and III represents a condensed sediment section and may contain a complete Holocene record of changing paleoenvironments, one that records the transition from a glacial, ice shelf environment to an open marine, Holocene environment. A sharp drop in magnetic susceptibility at mid-core is a common sedimentological feature of each basin. Presently, we favor a climate change hypothesis for this magnetic lithostratigraphic transition which may reflect the termination of the Holocene Hypsithermal and a marked change in productivity dated ca. 2500 years BP.

Keywords: Antarctica; Bellingshausen; climate; sedimentology

1. Introduction

The Antarctic Peninsula (Fig. 1) is an important area for paleoclimatic research because of its close proximity to the Antarctic Convergence and its polar to sub-polar climatic gradient (Griffith and Anderson, 1989; Domack and Ishman, 1992; Domack et al., 1995; Domack and McClennen, 1996). The varied sediments of the peninsula shelf and fjords indicate extended development of glaciers,

* Corresponding author. E-mail: mekirby@mailbox.syr.edu

0025-3227/98/$19.00
PII: S0025-3227(98)00043-7

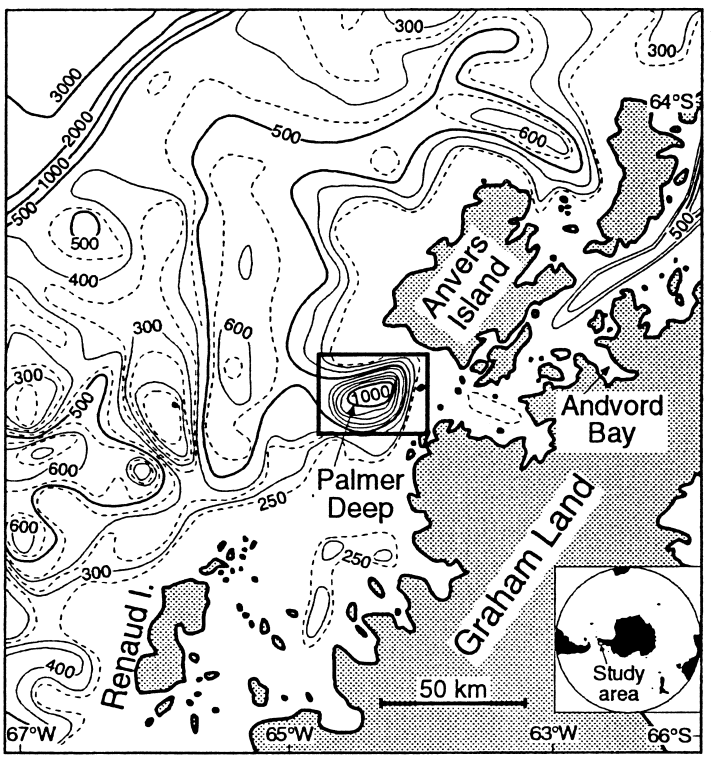

Fig. 1. Map of the Antarctic Peninsula and study location (after Rebesco et al., 1998b).

glacial recession, and subsequent paleoclimate evolution during the Holocene (Domack et al., 1991, 1993, 1995; Pope and Anderson, 1992; Pudsey et al., 1994; Bart and Anderson, 1995; Domack and McClennen, 1996). To date, research has focused upon two settings: the outer shelf (Pudsey et al., 1994; Vanneste and Larter, 1995; Larter and Vanneste, 1995) and fjords (Griffith and Anderson, 1989; Domack and Ishman, 1992; Domack et al., 1993, 1995; Domack and McClennen, 1996). It is hypothesized that during the Last Glacial Maximum (LGM) an expanded peninsula ice sheet (cap) reached the outer shelf where it deposited a series of prograding shelf edge clinoforms indicative of subglacial and proglacial sediment gravity flow deposition (i.e. till deltas, Larter and Vanneste, 1995). Recession from the LGM position is thought to have taken place at about 11,000 years BP (Pudsey et al., 1994) when ice drainage separated into individual valley tributaries. Each valley tributary drains ice from the elevated plateau of the peninsula (Domack and Ishman, 1992). Since the LGM, most siliciclastic deposition has been limited to fjord basins where sedimentation commenced as early as 9000 years BP (Shevenell et al., 1996).

Given the above context for glaciation across the peninsula shelf, it is surprising, considering the accessibility and research potential, that little work has been done on basins that mark an intermediary position between full glacial conditions (shelf edge grounding) and interglacial conditions (fjord head glaciation). We demonstrate herein and in a companion paper (Rebesco et al., 1998a) that basins such as the Palmer Deep (Fig. 2) contain relatively thick sediment accumulations (approximately 50–250 m) despite the long-standing assumption that such inner shelf areas were swept clean of interglacial deposits during subsequent glaciations (Barker, 1992).

This paper intends to describe the basic sedimentology and magnetic lithostratigraphy between a series of sediment piston cores from the Palmer Deep basins, discuss the nature of deep basin deposition on the inner shelf, establish a first-hand sediment chronology, and present a hypothesis to explain a

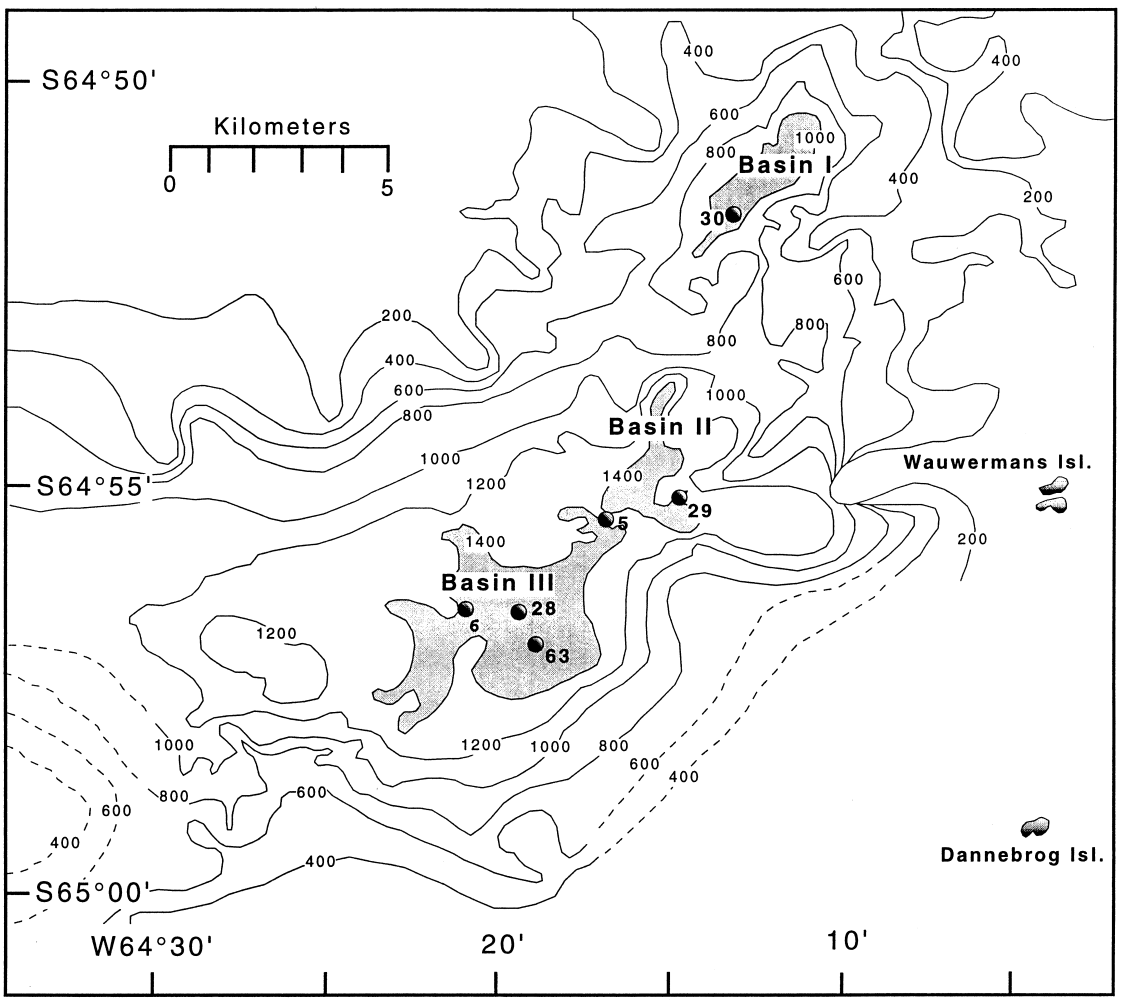

Fig. 2. Bathymetric map of the Palmer Deep with core locations.

sudden and pervasive MS modal change in each regional study core presented in this paper. Data used to address these questions were obtained during the *Polar Duke* 92-2 and *Deep Freeze* 1985 (USCGC *Glacier*) research cruises.

1.1. Basin description and core locations

The Palmer Deep area exhibits a complex, irregular, and unusually deep bathymetry (up to 1450 m) for a shelf environment (Fig. 2). We recognize and focus on three distinct basins: Basin I, Basin II, and Basin III (Fig. 2). Basin I (Fig. 2) is the shallowest basin with an estimated maximum depth of 1035 m. It is also the most northern of the basins occupying a perched position with respect to the deeper Basins II and III. A sill rises to 750 m depth along the south end separating Basin I from Basin II. Core PD92-30 was collected in the southwest end of Basin I (Fig. 2). Basin II (Fig. 2), located between Basins I and III, has an estimated maximum depth of 1415 m. An isolated basin floor high shoals to 1190 m in the southwest corner. Core PD92-29 was collected in the southeastern section of the basin floor; core PD92-5 was collected on the crest of a sill that separates Basin II from Basin III (Fig. 2). Basin III (Fig. 2), located furthest from Anvers Island (20 km southwest) but closest to the Dannebrog Islands (11 km west),

has an estimated maximum depth of 1450 m. This basin is also the largest of the three basins measuring approximately 26 km^2 in area. Cores PD92-28, PD92-06, and DF85-63 were collected in the central portion of Basin III (Fig. 2).

2. Methods and procedure

2.1. Bathymetry map

A new bathymetry map for the Palmer Deep basin was developed (Fig. 2) using data from Griffith (1988) and new 12-kHz precision depth records from the three RV *Polar Duke* cruises, 88-3, 90-7, and 92-2 (Kirby, 1993). Location and depth from the GPS and the PDR, respectively, were plotted at 15-min intervals along the cruise tracks on a map with interpolation between points (Kirby, 1993).

2.2. Palmer deep cores and analyses

Six sediment piston cores collected from the Palmer Deep are discussed in this paper (Table 1; Fig. 2). Core DF85-63 was obtained during the *Deep Freeze* 1985 research cruise (core 63 hereafter; see Table 1; Fig. 2). Cores collected during the *Polar Duke* 92-2 research cruise include PD92-06, PD92-28, PD92-05, PD92-29, and PD92-30 (cores 6, 28, 5, 29, and 30 hereafter; see Table 1; Fig. 2). Core 63 was analyzed by magnetic susceptibility (Fig. 3), ^{14}C dating (Table 2; Fig. 4), X-radiography, gravel grain counting (Fig. 5), smear slide counting (Fig. 5), percent biogenic silica (Fig. 5), and relative $CaCO_3$ content (Fig. 5). The remaining five cores were analyzed by core lithology (Fig. 6), magnetic susceptibility (Fig. 3), and sediment structure via X-radiography (Fig. 6).

Table 1
Core information

Core name and location	Length (cm)	Water depth (m)
PD92-05 64º55.472S, 64º16.631W	438	1410
PD92-06 64º56.532S, 64º20.755W	729	1440
PD92-28 64º56.501S, 64º19.484W	878	1430
PD92-29 64º55.107S, 64º14.431W	884	1400
PD92-30 64º51.720S, 64º12.506W	884	1040
DF85-63 64º56.9S, 64º19.0W	1105	1373

The MS was determined using a Bartington MS-2C magnetic susceptibility loop sensor (units in centimeter grams seconds [cgs $\times 10^{-6}$]). Whole core measurements were obtained for all cores except core 63 which was split prior to MS measurement accounting for the comparatively low values for this core because of the decrease in core volume (Fig. 3). Radiocarbon dates on acid insoluble organic matter were determined at the University of Arizona AMS facility. Ages were corrected based upon a $\delta^{13}C$ of 25‰, but were not adjusted for reservoir effects (see below; Table 2). Gravel grain counts on core 63 were conducted according to established procedures (Grobe, 1987; Domack et al., 1989). Smear slide analyses and percent biogenic silica data were used from Griffith (1988) and Liu et al. (1992), respectively; determination of biogenic silica followed that of DeMaster (1979). Relative $CaCO_3$ contents based on a scale of three, 3 being the most reactive and 0 being non-reactive, were determined with a 10% HCl solution on 2 cm^3 air-dried samples. Although qualitative and not standard procedure, such observations are significant to determine the presence or absence of $CaCO_3$ in sediments that typically lack any carbonate. Subsequent examination of carbonate bearing samples under a Scanning Electron Microscope revealed that the carbonate was detrital, in the form of fragmented bryozoan and molluscan skeletal debris, and was not associated with any identifiable nannoplankton (Claire Findlay, pers. commun., 1996).

3. Results and core description

3.1. Core description and analysis

Core DF85-63. Core 63, collected from Basin III (Fig. 2), consists predominantly of a homogeneous, bioturbated diatom mud and ooze (Liu et al., 1992). However several thin laminae of diatomaceous oozes and laminated sands were noted several years after the core was originally split and described. The gravel grain counts (from X-radiographs) show al-

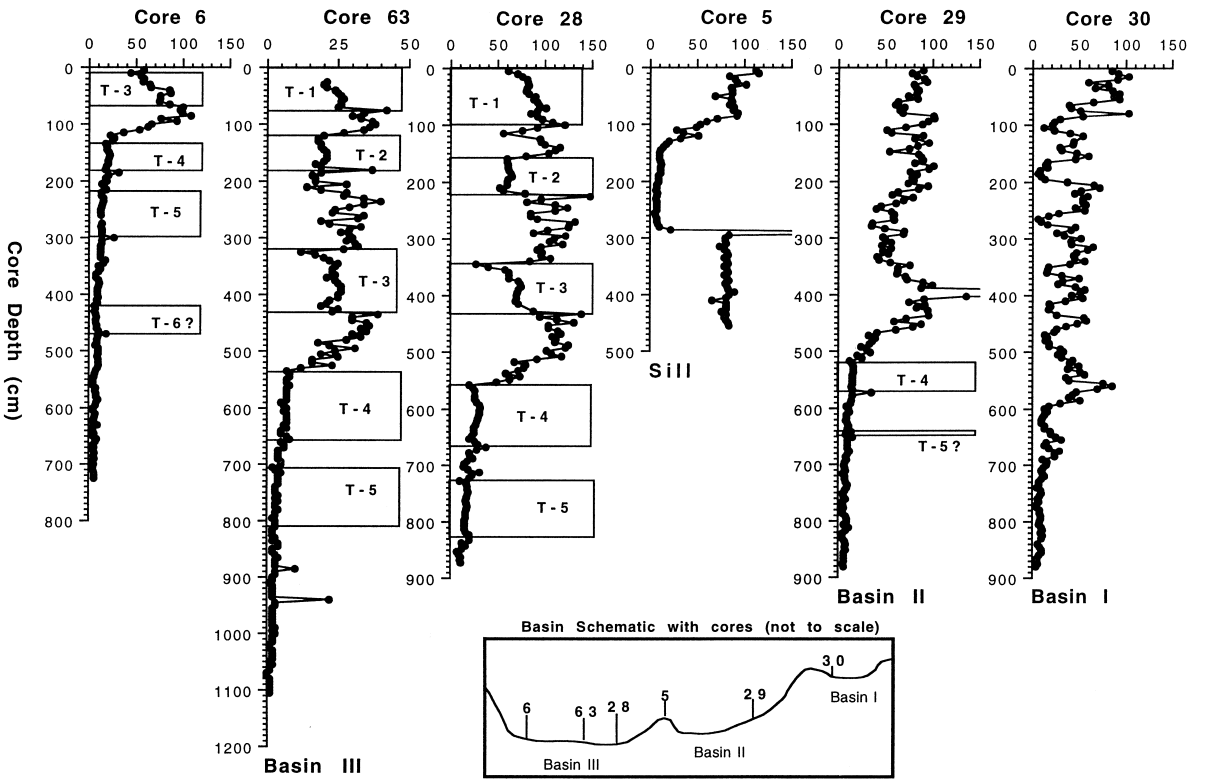

Fig. 3. Magnetic susceptibility (MS) (cgs $\times 10^{-6}$) for split core 63 and whole cores 6, 28 (Basin III), 5, 29 (Basin II), and 30 (Basin I). Turbidite units are indicated by *T*. Note the sharp decrease in MS values in cores 6, 63, 28, 29, and 30 and in the middle of core 5.

Table 2
Uncorrected radiocarbon ages (core DF85-63)

Lab No.	Core depth (cm)	Uncorrected age	Carbon source
AA-9037	65, T	3260 ± 120	POC
AA-9038	165, T	5690 ± 70	POC
AA-9040	282	3610 ± 75	POC
AA-9041	426, T	4265 ± 75	POC
AA-9042	565, T	5805 ± 75	POC
AA-9043	705, T	5585 ± 65	POC
AA-9044	865	5570 ± 100	POC
AA-9039	1005	6630 ± 75	POC

POC = particulate organic carbon, acid insoluble; T = date from turbidite unit.

ternating units of gravel-rich sediment and sediment without gravel (Fig. 5). Gravel-rich units average 5–7 grains per 5-cm interval.

The percentage biogenic silica shows a slight increasing trend with depth (Fig. 5). An anomalously high biogenic silica value (58%) occurs at 533 cm corresponding to a layer of diatom ooze. A number of the high biogenic silica values correlate with thin diatom ooze laminae, while a number of the low biogenic silica values correlate with sand laminae. The relative $CaCO_3$ reaction results show an increase in sediment reaction with core depth (Fig. 5). A transition in sediment reactivity to HCl from low to high occurs between 600 and 700 cm. Smear slide results show an increase in percent diatoms with core depth while the quartz percentages reveal a decrease with core depth (Fig. 5). This change occurs between 600 and 700 cm depth; however, the limited number of data points constrain any interpretation concerning rate of change. Magnetic susceptibility (Fig. 3) shows an abrupt change between higher, variable values above 520 cm to lower, uniform values below 530 cm. Average MS above 530 cm is 26 cgs $\times 10^{-6}$; MS values below 530 cm average 3.5–4 cgs $\times 10^{-6}$.

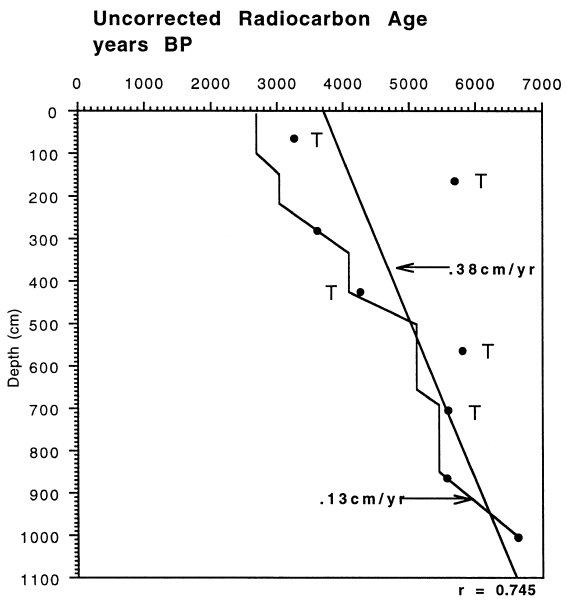

Fig. 4. Uncorrected AMS ^{14}C (bulk organics) versus depth for core 63 (see Table 2). Sedimentation rates were determined by best line fit for all data (regression line 0.38 cm/yr), and by extrapolation between ages determined for hemipelagic intervals (0.13 cm/yr) and instantaneous turbidite events in the core (solid line). *T* indicates samples from turbidite units.

The uncorrected ^{14}C data show a general increase in age with increasing core depth. ^{14}C dates have not been corrected for the carbon reservoir effect because of an unclear understanding of regional Antarctic ^{14}C reservoir age variability (Fig. 4; Table 2). Fig. 4 shows the sedimentation rate for the core as determined by dating both turbidite units and sections of pelagic/hemipelagic sediment; however, the presence of reworked organics in the turbidite units will affect the calculation of a standard linear fit line for determining a sedimentation rate. To accommodate this problem, we have determined two sedimentation rate models which consider both the turbidite units and the normal, pelagic/hemipelagic units as shown by the stepped, best-fit (dashed) lines in Fig. 4. This dualistic approach accounts for these turbidites as a naturally occurring, geologically instantaneous depositional feature. As a result, sedimentation rate estimates actually will be more accurate for the real depositional environment where turbidites are a natural part of the system. Therefore, this will allow for a better estimate of sediment thickness below the core base than estimates which do not consider turbidites. Taken separately each such interpretation results in a sedimentation rate of 0.13 and 0.38 cm/yr, respectively (Fig. 4). The latter rate is comparable to that determined for core 30 at 0.3–0.4 cm/yr (Leventer et al., 1996); however, core 30 is from Basin I, a shallower basin devoid of turbidites, thus we conclude that the actual sedimentation rate for Basin III lies somewhere in-between our estimated values.

Core PD92-5. All of the *Polar Duke* cores are described in some detail by Janecek et al. (1996). These descriptions vary somewhat from our own observations because we based our descriptions on freshly cut cores in which color differences served as important indicators of sedimentary units. The contrasts in sediment color last for only a few hours after exposure, and most cores from the basin presently have a homogenous appearance. The lithology of core 5 is shown as Fig. 6 and the MS as Fig. 3. Core 5 is located on a sill or bathymetric saddle between Basins II and III (Fig. 2).

Sediments in core 5 are composed of two types (Fig. 6): (1) laminated to thinly bedded, olive-green to dark olive-green mud with bioturbation and ice rafted debris throughout, and (2) olive-green, silty diatom mud with no coarse or poorly sorted material. The latter sediment type is rather homogenous, lacks bedding, and is devoid of bioturbation. A very thin-bedded unit with interlaminated, very fine-grained sand and mud is located at 290 cm denoting a sharp boundary, perhaps erosional, between two distinct and separate sediment facies (types 1 and 2 above, Fig. 6).

The magnetic stratigraphy (from top to bottom) illustrates a high, slightly variable MS unit between 0 and 100 cm, a middle, low MS unit between 100 and 290 cm, and a high but uniform MS unit below 290 cm (Fig. 3). The laminated unit type 1 as described above corresponds to the low MS unit (100–290 cm) and to the overlying high, slightly variable MS unit (0–100 cm). The interlaminated sand and mud layer denotes a MS maximum at 290 cm. The bottom, high but uniform MS unit (below 290 cm) is not laminated and lacks coarse-grained material.

Magnetic susceptibility (Fig. 3) shows a gradual change from higher values above 100 cm which

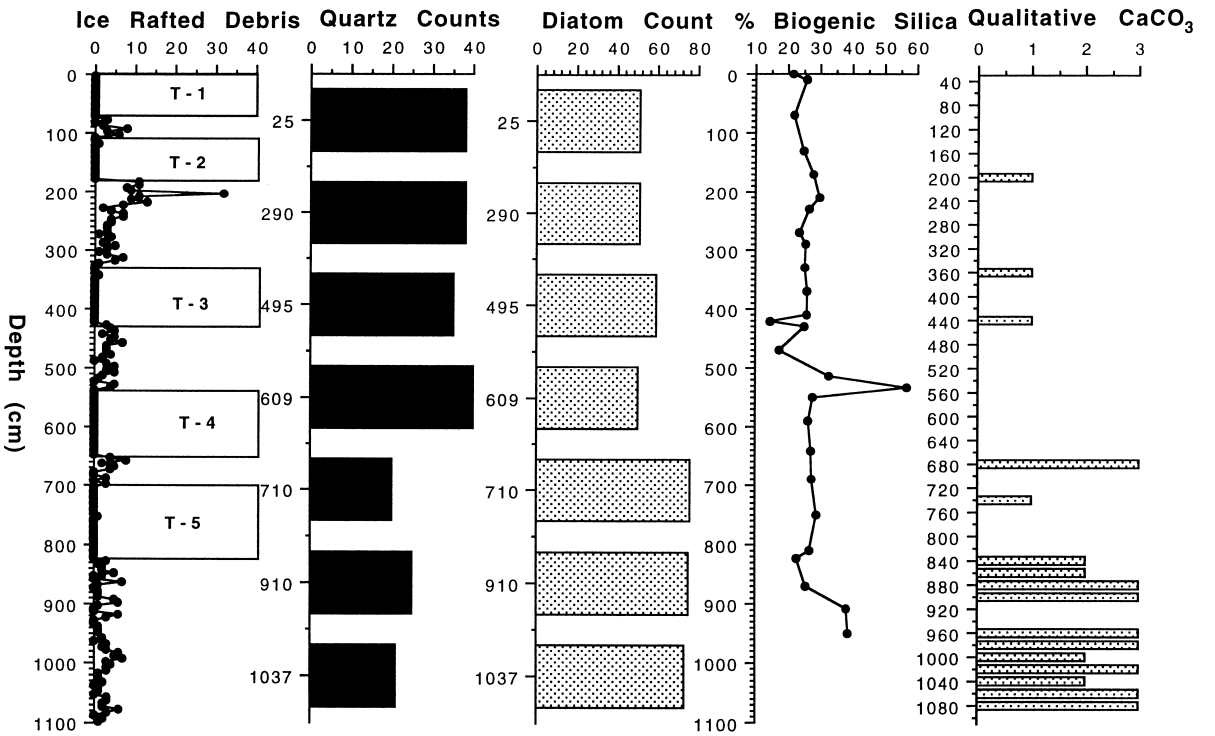

Fig. 5. Sedimentological data for core 63 include (from left to right): (1) gravel grains/5 cm core depth (IRD), (2) and (3) smear slide quartz versus diatoms (Liu et al., 1992), (4) % biogenic silica (from Griffith, 1988), and (5) qualitative $CaCO_3$ determination. Note the increase in biogenic content below 8 m as recognized in the three proxy records for paleo-productivity, diatoms, % biogenic silica, and $CaCO_3$. Turbidite units (*T*) are characterized by low to negligible IRD content.

average 88 cgs $\times$ 10^{-6} to lower, uniform values below 125 cm which average $<$10 cgs $\times$ 10^{-6}. An abrupt change from the lower, uniform MS unit to a high, uniform MS unit occurs at 285 cm; MS values from this bottom unit average 85 cgs $\times$ 10^{-6}.

Core PD92-6. Core 6 lithology and MS are shown as Figs. 3 and 6. Core 6 is located at the southern extremity of Basin III at a water depth of 1440 m (Fig. 2). It represents the deepest core site location from the Palmer Deep (Table 1). Sediments in core 6 are composed of two types (Fig. 6): (1) stratified, olive-green to dark olive-green mud with bioturbation and ice rafted debris throughout, and (2) homogenous, olive-green diatom mud overlain by a thin diatom ooze.

MS records show an upper unit with high, variable MS, between 0 and 120 cm and a lower section of very low, uniform MS, below 120 cm (Fig. 3). Three of the homogeneous, fining-upward diatomaceous mud turbidites (T-4, T-5, and T-?) are clearly identified by the MS data having slight MS maxima at their bases and uniform MS values within the intervening homogenous mud; the upper diatom mud unit, T-3, appears to be an exception to this observation. A significant upper portion of sediment from core 6 appears to be missing when compared to the remaining study cores; however, it is not clear if this effect is due to core over-penetration, lower sedimentation rates, or erosion.

Magnetic susceptibility (Fig. 3) shows a gradual change from high values above 80 cm to lower, uniform values below 120 cm. Average MS above 80 cm is 60 cgs $\times$ 10^{-6}; MS values below 120 cm average 12 cgs $\times$ 10^{-6}.

Core PD92-28. The lithology of core 28, also located in Basin III (Fig. 2), is shown as Fig. 6. Sediments in core 28 consist of two types: (1) stratified, olive-green to dark olive-green mud with bio-

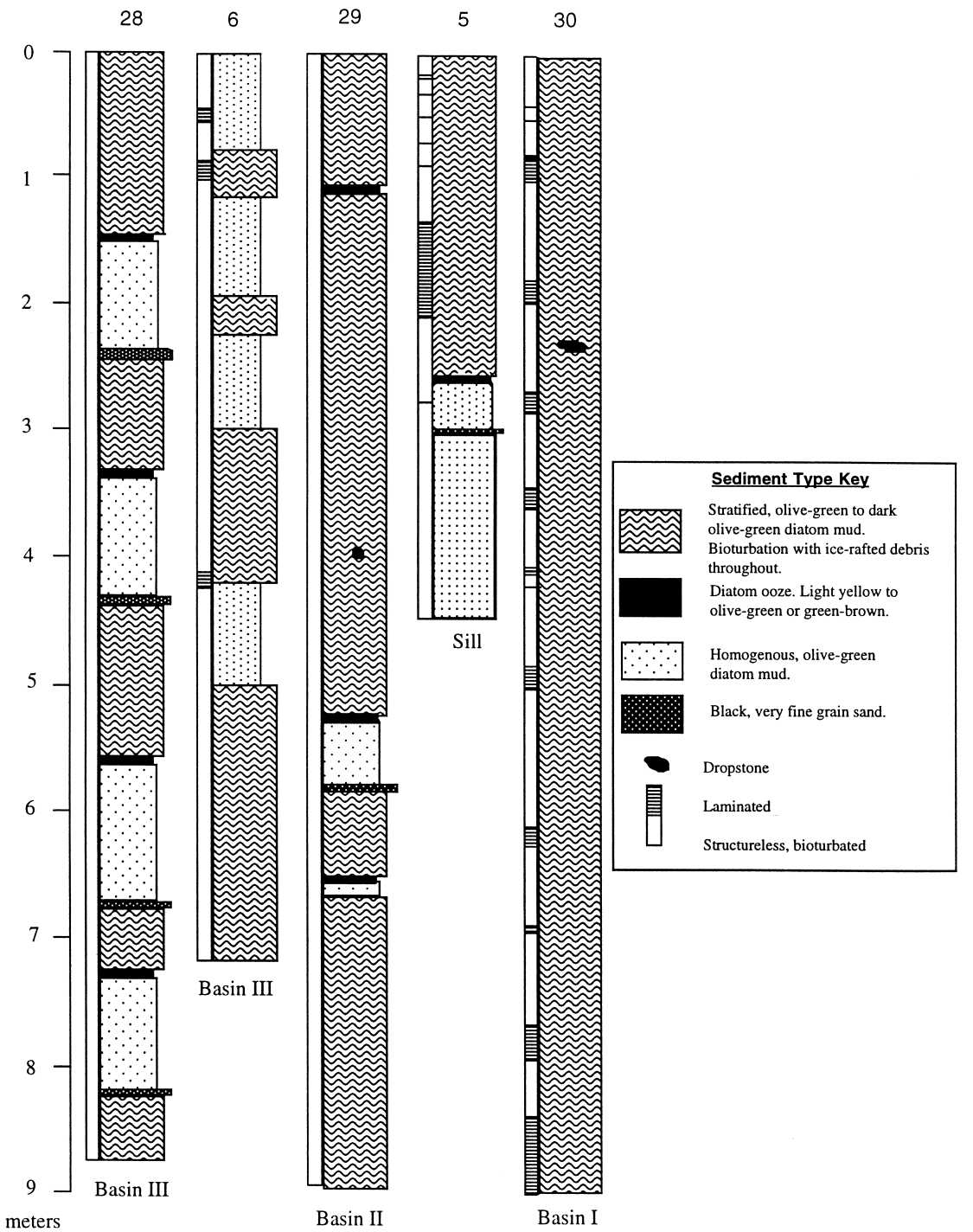

Fig. 6. Sediment descriptions for cores 5, 6, 28, 29, and 30. See Table 1 for core information.

turbation and ice rafted debris throughout, and (2) three-component units marked by a bottom layer of thin (1–2 cm) black, very fine sand, a middle layer (20–100 cm) of homogeneous, olive-green diatom mud, and a top layer of thin (1–2 cm) light-yellow to olive-green diatom ooze.

The similar MS stratigraphy between cores 28 and 63 provides for a suitable correlation between the five turbidite marker beds (T) (Fig. 3). Magnetic susceptibility (Fig. 3) shows an abrupt change from higher, variable values above 540 cm to lower, uniform values below 540 cm. Average MS above 540 cm is 80 cgs $\times$ 10^{-6}; MS values below 540 cm average 12–15 cgs $\times$ 10^{-6}.

Core PD92-29. The lithology of core 29, in Basin II (Fig. 2), is shown as Fig. 6. Sediments in core 29 consist of four types: (1) stratified, olive-green to dark olive-green mud with bioturbation and ice rafted debris throughout, (2) a three-component unit marked by a bottom layer of thin (1–2 cm), black very fine sand, a middle layer (20–100 cm) of homogeneous olive-green mud, and a top layer of thin (1–2 cm) light-yellow to olive-green ooze, (3) a two-component unit with a bottom layer of homogeneous, olive-green mud and a top layer of light yellow to olive-green ooze, and (4) green-brown diatom ooze. Sediment types 3 and 4 represent incomplete parts of a turbidite layer.

Magnetic susceptibility (Fig. 3) shows a gradual change from higher, fluctuating values above 450 cm to lower, more uniform values below 520 cm. Average MS above 450 cm is 72 cgs $\times$ 10^{-6}; MS values below 520 cm average 7–10 cgs $\times$ 10^{-6}.

Core PD92-30. Core 30, from Basin I (Fig. 2), lithology is shown as Fig. 6. Sediments in core 30 consist of one type: a stratified (laminated to thinly bedded), olive-green to dark olive-green mud to ooze with bioturbation and ice rafted debris throughout. Occasional 1 cm thick diatom ooze or very thin black sand laminae are also present.

Magnetic susceptibility (Fig. 3) shows a gradual change from higher, variable values above 570 cm to lower, uniform values below 600 cm. Average MS above 570 cm is 40 cgs $\times$ 10^{-6}; MS values below 600 cm average 7–10 cgs $\times$ 10^{-6}. Note that the MS values show cyclical fluctuations above 570 cm, on the scale of 40–60 cgs $\times$ 10^{-6}. Ten radiocarbon dates for core 30 are reported in Leventer et al. (1996) which date the MS decrease at ca. 2500 yr BP.; these data are not presented in this paper. Their results demonstrate an overall sedimentation rate of 0.2–0.4 cm/yr.

4. Discussion and interpretation

4.1. Sedimentology, MS lithostratigraphy, and deposition

Cores 63, 6, and 28 were extracted from the same deep portion of Basin III, seismically characterized by ponded infill (Fig. 1; Rebesco et al., 1998a). Fig. 6 illustrates the visual core descriptions. All three cores contain numerous (denoted as T1–T5) mud turbidites (Figs. 3 and 6). These turbidites are characterized by very thin, fine-grained sand layers at the base, grading into structureless, homogeneous diatom muds, capped with thin bioturbated diatomaceous oozes, although two cores, 6 and 29, contain incomplete turbidite sediment facies. X-radiographs clearly distinguish these turbidites by their complete lack of coarse gravel and/or ice rafted debris indicative of rapid deposition (Fig. 5). The low to intermediate MS values found in the turbidite units most likely reflect the influx of shelf sediments rich in organic material which dilute the MS signal. The intervening, interbedded, hemipelagic diatomaceous muds contain significant gravel suggesting that normal periods of hemipelagic deposition are characterized by regional ice rafting. Thin turbidite units in core 6 and the lack of basal sand units in these turbidites suggest that core 6 occupies a more distal sedimentary position with regard to turbidity currents than the sites of cores 28 and 63; this interpretation holds true for core 29 from Basin II as well (Fig. 3).

Core 5, which sits on the sill between Basins II and III, appears to lack any turbidite units; the only sorted sand in core 5 is an interlaminated layer separating the two major lithologic units of the core (Fig. 3). The magnetic stratigraphy in core 5 suggests that it represents a condensed section. It contains both the high, irregular MS unit at the top and the uniformly low MS unit in the middle, similarly found in the remaining study cores, in addition to a uniformly high MS unit at the bottom. The first two MS units are the only units found in the other

Palmer Deep cores; the third uniformly high MS unit is unique to core 5.

While this characteristic decrease in MS within all cores may reflect the diagenetic dissolution of magnetite with depth, iron-sulfur diagenesis controlled by higher carbon content in zones of increased productivity (Karlen, 1990; Tarduno, 1994; Leventer et al., 1996), or, as we suggest, signal attenuation or dilution via increased primary productivity as suggested by the correlative increase in floristic components (Leventer et al., 1996), the undisturbed laminated lithostratigraphy across the MS transitional zone in core 5, as well as all the study cores, clearly suggests that this MS change reflects a switch in a primary depositional environment for the study region as a whole which is not recorded as a lithologic change. Seismic profile analyses also support this hypothesis as indicated by the lack of a clear seismic profile change across the transitional MS zone (Kirby, 1993). The low MS unit in core 5 represents the only complete recovery of this unit from the Palmer Deep; this suggests that core 5 contains a longer, although lower resolved, paleoenvironmental record, extending below the recovered base of the other cores. The thin sand layer at 290 cm has a MS value >150 cgs, much higher than that measured in the other sand intervals for the study core region (Fig. 3). An analysis of visual core lithology and X-radiography clearly excludes this sand layer as the basal layer of a turbidite facies due to the abrupt and permanent shift in sediment facies type above and below 290 cm. Since other sand layers from the study cores denote the base of turbidite units, the anomalously high MS sand layer in core 5 at 290 cm implies a change in sand provenance, primary depositional process, or a possible depositional hiatus. We have interpreted the sand layer at 290 cm as the initial depositional product of a regional paleoenvironmental change, perhaps a transition between a glacial, ice shelf environment to the modern open water, Holocene environment. The former paleoenvironment may account for the lack of bioturbation in this bottom, uniformly high MS unit.

In Basin II, turbidity currents are not as prevalent; basin infill consists of both ponding and drape (Rebesco et al., 1998a). Core 29 contains two, very thin mud turbidites (Figs. 3 and 6), both at core depths greater than 5 m and within the low MS unit. Turbidites 4 and 5 are the thickest units in cores 63 and 28 and have been interpreted as possible correlatives to the only distinct turbidites (T-4 and T-5) observed in Basin II, core 29 (Fig. 3). The relative dearth of turbidite units in core 29 makes the magnetic stratigraphy less likely to have been disturbed, possibly reflecting subtle depositional variations for the region. Rapid changes in sediment deposition between biogenic-rich (siliceous) and siliciclastic-rich units are indicated in the upper 350 cm of core 29 by the stratified nature of the diatom mud and ooze units (Fig. 6), a similar sedimentological feature as observed in core 30 from Basin I (Leventer et al., 1996). A broad high in MS between 350 and 450 cm may reflect a dominance of hemipelagic sedimentation and ice rafting between short periods of enhanced biogenic productivity.

The differences in sedimentation between Basins II and III is striking given their close proximity and similar depths. The saddle between the two basins is less than 50 m high, but, as observed by the distribution of turbidites, it provides a significant boundary between two distinct depositional environments. Cores 6, 28, and 63, from Basin III, reflect a deposystem dominated by occasional turbidity currents and longer periods of alternating pelagic/hemipelagic sedimentation. Core 29, from Basin II, reflects a deposystem dominated by pelagic/hemipelagic sedimentation with rare turbidity currents (Figs. 3 and 6). A combination of seismic profile analyses gathered during the *Polar Duke* 92-2 cruise and sedimentation rate extrapolations from this study clearly indicates that the sediments within Basins II and III extend through the Holocene, even considering the effect of turbidites, depositional hiatuses, and varied glaciomarine sedimentological processes (Kirby, 1993).

Basin I, located just north-northeast from Basins II and III, provides an excellent depositional setting for undisturbed, high-resolution sediment records because turbidite units are not present. The absence of turbidite units in Basin I suggests that the proposed turbidity current pathways (from the basin side walls based on seismic profile analyses; Kirby, 1993) for Basins II and III do not affect Basin I. Core 30 (Figs. 3 and 6) illustrates the well-stratified nature of the sediments; this is supported by seismic analysis (Kirby, 1993; Rebesco et al., 1998a). As with cores 5, 6, 63, 28, and 29, a decrease in MS values

occurs at mid-depth (580 cm) in core 30. Unlike the other cores, however, there is a clear alternating (cyclical) pattern recorded by the MS in the upper 570 cm of core 30 (Fig. 3). The cyclic nature of the MS signal reflects a change in the dominant form of sediment being deposited (Leventer et al., 1996). Periods of high MS reflect a hemipelagic environment rich in siliciclastic, terrigenous material, particularly silts and clays (Leventer et al., 1996). The low MS units denote a depositional environment dominated by pelagic, biogenic (siliceous) sedimentation, reflecting an increase in regional productivity that reoccurs on a multi-century time scale (Leventer et al., 1996). Thus, the cyclic nature of the sediments from Basin I and Basin II, prior to the MS decrease, truly reflects a regional climatic change at a high level of resolution. The base of core 30 dates to ~4 ka radiocarbon years and hence by extrapolation the bottom of the basin's infill, based on seismic profiles, is estimated to be ~15 ka.

4.2. Chronology and mid-core MS change.

The magnetic stratigraphy outlined in Fig. 3 is tied to the radiocarbon time scale in cores 63 and 30. Using the ages indicated in Table 2 and discussed by Leventer et al. (1996), we conclude that cores 63, 28, 29, and 30 represent the middle to late Holocene. Cores 6 and 5 extend beyond this, most likely into the early Holocene and probably, in the case of core 5, into the Late Pleistocene. The low MS unit at the base of all the study cores and found in the middle of core 5 likely marks the Holocene climatic optimum, or Hypsithermal, roughly between 8 and 2.7 ka. This is consistent with other glacial marine records from the Antarctic Peninsula (Shevenell et al., 1996), the Ross Sea (Jacobson, 1997), and Wilkes Land (Harris et al., 1998); however, a better age constraint is required and pending for our study. The lower MS values determined in this unit reflect dilution via increased primary productivity. An increase in % biogenic silica and $CaCO_3$ reaction in addition to a decrease in quartz support a hypothesis for a more productive mid-Holocene (Hypsithermal) for the region as represented by the first-order MS change for all of the study cores (Figs. 3 and 5). Diagenetic dissolution of magnetite is an unlikely explanation for the MS decrease because of the highly varied core depth at which the MS change occurs; we would expect a similar depth change if diagenesis had occurred. The striking increase in MS values for all the study cores may reflect the termination of the Holocene Hypsithermal and a significant decrease in regional productivity dated at ca. 2500 years BP (Leventer et al., 1996). As a result, the hemipelagic sediment background MS signal is enhanced via minimal dilution by organic material. Clearly, the magnetic lithostratigraphy used for this study provides a powerful, first-order methodology for extracting and correlating regional lithostratigraphic change possibly linked to climate as we suggest here.

5. Conclusions

The data collected and analyzed for this project led to the following conclusions.

The Palmer Deep bathymetry is complex, divided into three basins, each recording an unique sedimentological history.

Five to six mud turbidites are found within Basins II and III, but not in the shallower Basin I. These turbidites most likely originate from the respective basin side walls and shelf environments, although provenance studies have not been conducted to confirm this statement.

The magnetic susceptibility decreases to low, almost negligible, values below mid-core (4–6 m) for each of the cores collected, suggesting a regional depositional and environmental change dated at approximately 2500 years BP or the end of the Holocene Hypsithermal.

Decreases in the percent biogenic silica, $CaCO_3$, and diatomaceous sands seen in core 63 slightly precede in core depth that of the MS increase; accurate measurements of time correlativity remain unclear because of the turbidite units. This observation indicates a potential time-response lag between processes controlling bioproductivity and the consequent change in primary sedimentation processes. We interpret this observation to indicate a climatic cooling with reduced biogenic marine productivity which continues to this day; this hypothesis is corroborated by the work of Leventer et al. (1996). This change towards a colder climate with lowered primary productivity has produced a hemipelagic signal

with higher MS values due to reduced dilution affects. During warmer periods prior to 2500 years BP, this hemipelagic component was diluted by the higher marine biogenic productivity and consequent organic matter flux.

Sediment studies from closed basins, such as the Palmer Deep, clearly indicate the potential for high-resolution, regional paleoclimatic studies along the Antarctic Peninsula for the late-glacial, Holocene transition and the Holocene itself.

Acknowledgements

This work was supported by the National Science Foundation (Office of Polar Programs–Ocean Sciences) through their Research in Undergraduate Institutions program (OPP 89-15977). We thank the crew of the RV *Polar Duke* and the staff of Antarctic Support Associates for their enthusiastic assistance of the field program. Constructive reviews by D.G. Masson, T. Van Weering, and two anonymous reviewers are appreciated. We thank the careful work of Claire Findlay (IASOS, Univ. Tasmania) who examined samples under the Scanning Electron Microscope facility at Antarctic Division, Kingston, Tasmania. Support of the PEW charitable trust is also acknowledged.

References

Barker, P.F., 1992. The sedimentary record of Antarctic climate change. Philos. Trans. R. Soc. London 338, 259–267.

Bart, P.J., Anderson, J.B., 1995. Seismic record of glacial events affecting the Pacific margin of the northwestern Antarctic Peninsula. In: Cooper, A.F., Barker, P.F., Brancolini, G. (Eds.), Geology and Seismic Stratigraphy of the Antarctic Margin. Antarct. Res. Ser. 68, 75–96.

DeMaster, D.J., 1979. The Marine Budgets of Silica and ^{32}Si. Ph.D. Thesis, Yale University, New Haven, CT.

Domack, E.W., Ishman, S.E., 1992. Magnetic susceptibility of Antarctic glacial marine sediments. Antarct. J. U.S. 27, 64–65.

Domack, E.W., McClennen, C.E., 1996. Accumulation of glacial marine sediments in fjords of the Antarctic Peninsula and their use as Late Holocene paleoenvironmental indicators. In: Ross, R., Hoffman, E., Quetin, L. (Eds.), Foundations for Ecosystem Research West of the Antarctic Peninsula. Antarct. Res. Ser. 70, 257–272.

Domack, E.W., Jull, A.J.T., Anderson, J.B., Linick, T.W., 1989. Application of tandem accelerator mass-spectrometer dating to late Pleistocene–Holocene sediments of the East Antarctic continental shelf. Quat. Res. 31, 277–287.

Domack, E.W., Jull, A.J.T., Nakao, S., 1991. Advance of East Antarctic outlet glaciers during the Hypsithermal: implications for the volume state of the Antarctic ice sheet under global warming. Geology 19, 1059–1062.

Domack, E.W., Mashiotta, T.A., Burkley, L.A., Ishman, S.E., 1993. 300 year cyclicity in organic matter preservation in Antarctic Fjord sediments. Antarct. Res. Ser. 60, 265–272.

Domack, E.W., Ishman, S.E., Stein, A.B., McClennen, C.E., Jull, A.J.T., 1995. Late Holocene advance of the Muller Ice Shelf, sedimentologic, paleontologic, and geochemical evidence. Antarct. Sci. 7, 159–170.

Griffith, T.W., 1988. A Geological and Geophysical Investigation of Sedimentation and Recent Glacial History in the Gerlache Strait Region, Graham Land, Antarctica. M.A. Thesis, Rice University, Houston, TX, 449 pp.

Griffith, T.W., Anderson, J.B., 1989. Climatic control on sedimentation in bays and fjords of the northern Antarctic Peninsula. Mar. Geol. 85, 181–204.

Grobe, H., 1987. A simple method for the determination of ice-rafted debris in sediment cores. Polarforschung 57 (3), 123–126.

Harris, P.T., Taylor, F., Domack, E.W., DeSantis, L., Goodwin, I., Quilty, P.G., O'Brien, P.E., 1998. Glacimarine siliciclastic muds from Vincennes Bay, East Antarctica; preliminary results of an exploratory cruise in 1997. Terra Antarct. (in press).

Jacobson, E.A., 1997. Ice Shelf Sedimentation and the Holocene Climatic Optimum in the Ross Sea, Antarctica. BA Thesis, Hamilton College, Clinton, NY, 67 pp.

Janecek, T.R., Curren, M., Domack, E.W., Hovan, S., Manley, P., 1996. Descriptions of sediment recovered by the R/V *Polar Duke*, United States Antarctic Program Cruise II, 1992, Antarctic Peninsula. Antarctic Marine Geology Research Facility, Florida State University, Tallahassee, FL, Contrib. 4, 95 pp.

Karlen, R., 1990. Magnetite diagenesis in marine sediments from the Oregon continental margin. J. Geophys. Res. 95, 4405–4419.

Kirby, M.E., 1993. High Resolution Seismic Stratigraphy and Sedimentology of Holocene Glacial Marine Deposits in the Palmer Deep, Bellingshausen Sea, Antarctica. B.A. Thesis, Hamilton College, Clinton, NY, 60 pp.

Larter, R.D., Vanneste, L.E., 1995. Relict subglacial deltas on the Antarctic Peninsula outer shelf. Geology 23, 33–36.

Leventer, A., Domack, E.W., Ishman, S.E., Brachfeld, S., McClennen, C.E., Manley, P., 1996. Productivity cycles of 200–300 years in the Antarctic Peninsula region: understanding linkages between the sun, atmosphere, oceans, sea ice and biota. Geol. Soc. Am. Bull. 108, 1626–1644.

Liu, X., Sun, D.C., Kelly, F.A., Kaharoeddin, F.A., Painer, C.J., Bryan, J.R., 1992. Descriptions of sediments recovered by the USCGC *Glacier* Operation Deep Freeze 1985, Bransfield Strait, Gerlache Strait, Marguerite Bay. F.S.U. Sedimentology Research Laboratory Contribution 55, 106 pp.

Pope, P.G., Anderson, J.B., 1992. Late Quaternary glacial history of the northern Antarctic Peninsula's western continental shelf: evidence from the marine record. Antarct. Res. Ser. 57, 63–91.

Pudsey, C.J., Barker, P.J., Larter, R.D., 1994. Ice sheet retreat

from the Antarctic Peninsula continental shelf. Cont. Shelf Res. 14, 1647–1675.

Rebesco, M., Camerlenghi, A., DeSantis, L., Domack, E.W., Kirby, M.E., 1998a. Seismic stratigraphy of Palmer Deep: a fault bounded late Quaternary sediment trap on the inner continental shelf, Antarctic Peninsula Pacific margin. Mar. Geol. 151, 89–110.

Rebesco, M., Camerlenghi, A., Zonolla, C., 1998b. Bathymetry and morphogenesis of the continental margin west of the Antarctic Peninsula. Terra Antarct. (in press).

Shevenell, A.E., Domack, E.W., Kernan, G.M., 1996. Record of Holocene paleoclimate change along the Antarctic Peninsula: evidence from glacial marine sediments, Lallemand Fjord. In: Banks, M.R., Brown, M.Y. (Eds.), Climate Succession and Glacial Record of the Southern Hemisphere. Papers and Proceedings of the Royal Society of Tasmania, Vol. 130, Pt. 2.

Tarduno, J., 1994. Temporal trends of magnetic dissolution in the pelagic realm: Gauging paleoproductivity? Earth Planet. Sci. Lett. 123, 39–48.

Vanneste, L.E., Larter, R.D., 1995. Deep-towed boomer survey on the Antarctic Peninsula margin: an investigation of the morphology and acoustic characteristics of late Quaternary sedimentary deposits on the outer continental shelf and slope. Antarct. Res. Ser. 68, 97–121.